Neutron scattering in ^{140,142}Ce and strengths of neutrons and protons in collective levels of ^{140}Ce

Gang Chen,* Min Li,† J. L. Weil, and M. T. McEllistrem
Department of Physics and Astronomy, University of Kentucky, Lexington, Kentucky 40506
(Received 22 July 1999; revised manuscript received 20 July 2000; published 19 December 2000)

Differential cross sections for 7.5 MeV neutron scattering from ^{140,142}Ce have been measured and analyzed in conjunction with previously known total cross sections between 0.5 and 10 MeV and scattering properties in the very low-energy or resonance region. The differential elastic scattering cross sections, total cross sections, and resonance-region properties enable us to fix the mean scattering fields, so that the scattering amplitudes at the nuclear surface are given with confidence. The inelastic scattering cross sections are then analyzed to extract the excitation strengths of a few collective levels. The level-excitation strengths found in this neutron scattering analysis provide insight into the 4_1^+ level's configuration, and also have been compared to strengths observed in electron scattering and Coulomb excitation to separate the roles of protons and neutrons in 2^+, 3^-, and 4^+ levels excited in ^{140}Ce.

DOI: 10.1103/PhysRevC.63.014606 PACS number(s): 25.40.Dn, 25.40.Fq, 27.60.+j, 28.20.Cz

I. INTRODUCTION

The goals of this experiment were the determination of the mean neutron scattering fields of the Ce nuclei and the mixture of isospin changes $\Delta I = 0,1$ in transitions from the ground states of ^{140}Ce to collective excited levels. Neutron scattering strengths to these levels are compared to those found in electromagnetic excitation, or those found from level lifetimes, to assess the isospin mixtures of the transitions. These mixtures then indicate the separate roles of target neutrons and protons in the levels excited. The levels to which scattering is observed are presented in Fig. 1; all have well established spins and parities.

In the case of $^{140}Ce_{82}$ only valence protons are present, so one can test the application of models which are based on the assumption that the low-lying levels are almost exclusively proton excitations. The quasiparticle phonon model (QPM) [1–4] was successfully used to describe level energies and transition rates in ^{140}Ce [3] based on this presumption.

Our experiments determined differential neutron scattering cross sections for elastic scattering in both nuclei and inelastic scattering in ^{140}Ce at an incident neutron energy of 7.5 MeV. Measurements were carried out at the 7 MV accelerator laboratory of the University of Kentucky. The elastic scattering cross sections were combined with known [5] total cross sections over an extended energy range and with resonance energy (eV region) scattering properties [6] to obtain a satisfactory mean field description of neutron scattering from the Ce nuclei. The mean field analysis was carried out within both a spherical optical model (SOM) formalism and a coupled channels (CC) formalism.

The SOM analysis is a simple one, and permits easy determination of a scattering field appropriate to the nucleus. It also permits the inclusion of calculations of cross sections attributed to compound system formation through the absorption represented by the imaginary part of the scattering potential. The CC formalism is designed specifically to account for those few excited levels whose scattering channels are strongly coupled to the elastic scattering channels. That formalism is used to analyze cross sections for strongly coupled levels in order to determine the direct excitation amplitudes to those levels. These amplitudes are a primary focus of this work.

Neutron scattering, as a probe of collective excitation strengths of nuclei, has the disadvantage of low incident flux which leads to the need for large scattering samples. The large samples together with the need to have a reasonable neutron flux also forces the energy spread in the experiments to be relatively large. But the advantage of neutron scattering is in the large range of scattering properties available to assist in determining a high confidence scattering potential or energy-dependent mean field. That description serves as a firm basis for examining inelastic excitation strengths. Coulomb excitation or electron scattering also provides excitation amplitudes, so that when neutron scattering and electromagnetic excitation are combined to separate isoscalar and isovector excitation amplitudes, or to separate target neutron and proton roles, that separation can be well determined.

II. EXPERIMENTAL METHODS

The methods for detecting scattered neutrons are those of a standard time-of-flight (TOF) detection system. These methods are well described in Ref. [7], and references therein. Therefore only a brief overview will be offered here.

A. Neutron source and scattering samples

The 7.5 MeV neutrons were produced via the ^{2}H$(d,n)^3$He reaction using a pulsed beam from the University of Kentucky 7 MV accelerator. The accelerator operated with a pulsing frequency of 1.875 MHz and produced an average beam current of 2.5 μA with deuteron pulses having a width of $\sim$1 ns. To minimize time spreading of the neutron

*Present address: Lightyear Communications, 1901 East Point Parkway, Louisville, KY 40223.
†Present address: Lexmark International, 740 W. New Circle Road, Lexington, KY 40511.

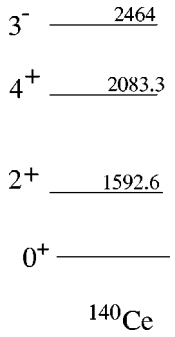

FIG. 1. The levels in ^{140}Ce excited strongly in neutron scattering. Excitation energies are given in keV.

bursts, a deuterium gas cell of 1.1 cm length and 0.8 cm diameter was employed. The gas cell was isolated from the accelerator vacuum by a 3.5 μm thick Mo foil. The gas cell pressure was 1.9 b, or almost two atmospheres.

Two scattering samples were used. One was a natural Ce cylinder with a mass of 48.34 g in a thin-walled steel container, 2.54 cm diam. by 2.5 cm height. The second sample was isotopically enriched in ^{142}Ce to 94% in the form of CeO_2 powder encased in a thin-walled polyethylene container. This sample contained 36.1 g of ^{142}Ce; it was on loan from the Isotopes Distribution Center of Oak Ridge National Laboratory. The natural sample of Ce metal served reasonably well as a ^{140}Ce sample, since its natural abundance is 88.4%. The other main constituent in the metal sample was ^{142}Ce, with 11.1% abundance. By comparing the elastic scattering differential cross sections for ^{142}Ce with those for the natural sample, it was observed that isotopic corrections to the data for the natural sample would be insignificant for elastic scattering. Two background samples were also used. One, used as background for the ^{nat}Ce runs, was a thin-walled steel container of the same size as the container for the natural Ce sample The other was a thin-walled polyethylene sample containing an amount of water such that the number of oxygen atoms in both the water and the enriched CeO_2 sample were the same.

In spite of the effort to obtain a good oxygen subtraction sample, the scattering from oxygen was so large that it was not feasible to obtain good data on excited levels of ^{142}Ce. The two to one ratio of oxygen to Ce atoms and the large oxygen scattering peak badly hindered the amount of data we could obtain for this nucleus, other than for elastic scattering. A natural carbon sample was used as a secondary standard for cross section normalization, since its elastic scattering cross sections are well known [8].

B. Neutron detection methods

Scattered neutrons were detected with a scintillator mounted in a large Li_2CO_3 loaded paraffin shield with Pb and steel inserts. The detector was set at a distance of 3.93 m from the scattering sample. The detector and its shield were mounted on a rotatable carriage centered on the scattering sample.

The main neutron detector was an 11.5 cm diam. by 2.5 cm thick NE-218 liquid scintillator with pulse-shape discrimination capabilities. Such a detector has an energy dependent efficiency, which was determined by measuring the angular distribution of neutrons from the source, and comparing detected yields to the well known angular distributions for this source reaction [9]. As in most neutron scattering experiments, the detector's acceptance bias is fixed by setting a window on the recoil proton spectrum in the scintillator. This detector was operated in the dynamic biasing mode developed by Brandenberger and Grandy [10]. This means that the recoil proton pulse height acceptance window was dynamically adjusted to correspond to the neutron energy being detected. The neutron energy being detected was inferred from the flight-time of neutrons from the source through the scatterer to the detector.

The most important contribution to the neutron energy spread came from the angular spread of neutrons incident on the scattering samples from the ^{2}H$(d,n)^3$He reaction, owing largely to the size of the sample. Other contributions came from the time dispersion of neutrons in beam pulses, and time dispersion in the neutron detector. The overall energy spread in the measurements was 220 keV.

The neutron source-to-sample distance was the most critical dimension of the detection geometry. Sample position was accurately maintained in spite of frequent sample

TABLE I. The energy dependent real and surface absorptive potentials for the SOV analyses of 7.5 MeV scattering of neutrons by the ^{140,142}Ce nuclei. See the caption of Table II for parameter definitions.

^{140}Ce		
	$V=47.07+0.01E$	$(0.5\leqslant E<3.5$ MeV$)$
	$47.81-0.2E$	$(3.5\leqslant E\leqslant 10$ MeV$)$
	$W_d=4.29+0.24E$	$(0.5\leqslant E\leqslant 10$ MeV$)$
^{142}Ce		
	$V=44.68+0.1E$	$(0.5\leqslant E<5.0$ MeV$)$
	$49.18-0.8E$	$(5.0\leqslant E\leqslant 10$ MeV$)$
	$W_d=3.69+0.24E$	$(0.5\leqslant E\leqslant 10$ MeV$)$

TABLE II. The potential parameter values at 7.5 MeV energy for both the SOM and SOV calculations. V is the depth of the real part of the Woods-Saxon potential, W_d is the depth of the surface absorption potential, V_{SO} is the depth of the spin-orbit potential, R_r is the real potential radius in fm, R_{WD} is the radius of the surface absorption, and R_{SO} is the radius of the spin-orbit term. The radii are obtained as $R_xA^{1/3}$. The a's are the diffusenesses of the respective potentials. The potential depths are in MeV and the radii and diffusenesses are in fm.

	V	W_d	V_{SO}	R_r	R_{WD}	R_{SO}	a_r	a_{WD}	a_{SO}
The SOM model									
^{140}Ce	48.9	3.26	5.0	1.24	1.21	1.17	0.62	0.58	0.58
^{142}Ce	45.9	6.9	5.5	1.30	1.21	1.06	0.51	0.49	0.37
The SOV model									
^{140}Ce	46.3	6.1	5.0	1.24	1.21	1.15	0.59	0.55	0.58
^{142}Ce	43.2	5.5	4.9	1.29	1.23	1.06	0.52	0.51	0.21

TABLE III. The coupling parameters $\beta_l^{n,n'}$ from neutron scattering and the interaction radii for neutron scattering are shown. The reduced $E2$ transition probabilities, which are the same from both electromagnetic decay rates and from electron scattering and the coupling strengths extracted from the $B(E2)$ values and from neutron inelastic scattering are given also.

	$\beta_l^{n,n'}$	R (fm)	$B(EL)$ $(e^2\,b^l)$	δ^{em} (fm)	$\delta^{n,n'}$ (fm)
^{140}Ce					
2^+	0.08	6.428	0.30±0.008	0.66±0.008	0.51±0.04
3^-	0.10	6.428	0.20±0.01	0.90±0.03	0.64±0.07
4_1^+	0.07	6.428	0.034±0.004	0.62±0.04	0.44±0.07

changes. The sample position was sighted with a fixed, high magnification telescope at 0°, with samples mounted in a wire harness suspended from a post at a fixed distance from the source. The distance from the center of the 1.1 cm long source to the center of the samples was maintained at 8.1 cm; repositioning accuracy was ±0.6 mm.

The incident neutron fluence was monitored by an 4.0 cm diam by 5.5 cm thick NE-218 scintillator mounted at a fixed location above the reaction plane, at 6.05 m from the neutron source and at an angle from the incident beam direction of 43.5°.

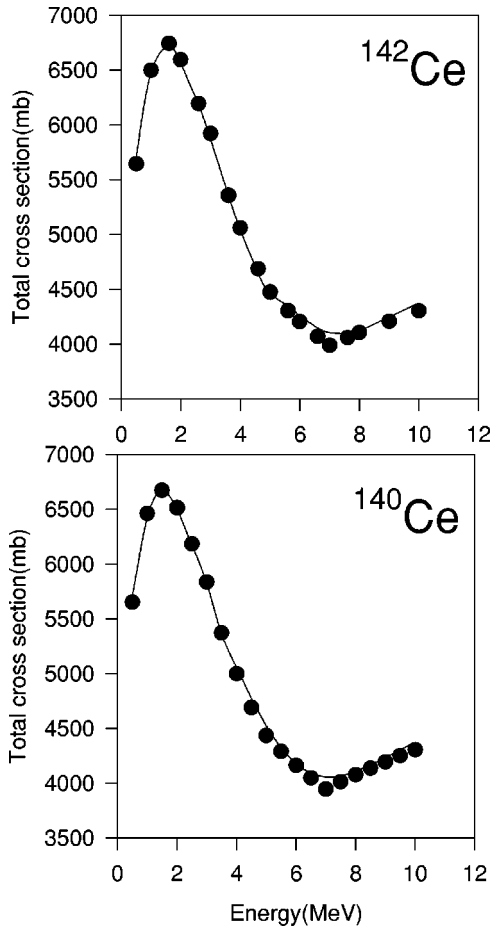

FIG. 2. Total cross sections for the two Ce isotopes from 0.5 to 10.0 MeV. The curves are SOV calculations and the data are from the ENDF-B/VI compilation of NNDC.

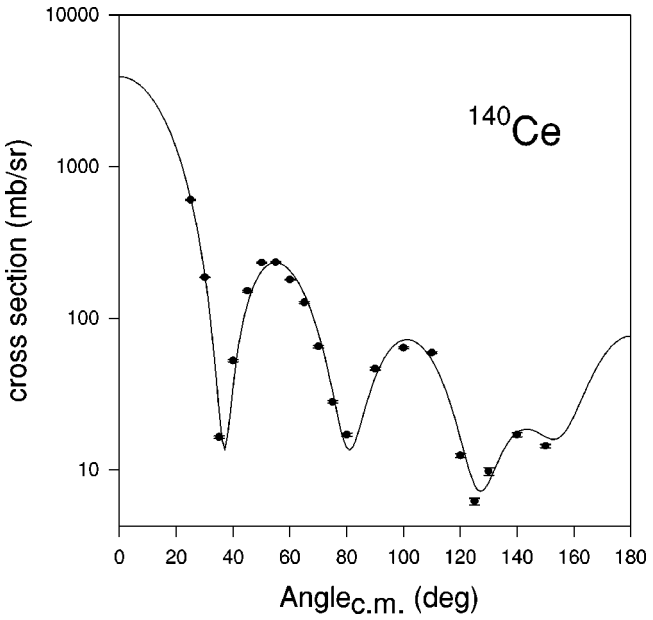

FIG. 3. Elastic scattering from ^{140}Ce at 7.5 MeV energy. The solid curve is a second order vibrational calculation.

C. Yield corrections and uncertainties

The yields obtained from peaks in the TOF spectra were extracted with a peak-fitting program [7], and corrected for neutron attenuation and multiple scattering in the sample with the forced collision Monte Carlo program MULCAT [11]. After normalization to the carbon scattering cross sections, using the same peak extraction and yield correction procedures for the carbon scattering yields as for the Ce yields, the experimental differential scattering cross sections were ready for interpretation via either SOM or CC formalisms.

Uncertainties of the differential scattering cross sections arise from several sources.

Statistical uncertainties are combined with peak fitting uncertainties using the TOF asymmetric peak fitting program SAN12 [7]. These uncertainties are well under ±1% for the strong peaks of elastic scattering, but averaged ±13% for scattering to the 2_1^+ level, ±20% to the 3_1^- level, and ±30% for those to the 4_1^+ level.

The neutron-fluence monitor yields were very large and well fit; the uncertainty is $\ll \pm 1\%$.

The energy dependence of the main neutron detector efficiency had an uncertainty of ±0.8%.

The Monte Carlo corrections for attenuation and multiple scattering have $< \pm 0.3\%$ uncertainty for elastic scattering, where large numbers of histories are available. But for inelastic scattering, with smaller numbers of histories in the Monte Carlo results, the uncertainty was about ±7%.

The relative uncertainties of the differential elastic scattering yields from the carbon normalization sample were ±0.7%, and the absolute normalization for the angle-integrated carbon elastic scattering cross section was ±3% [9].

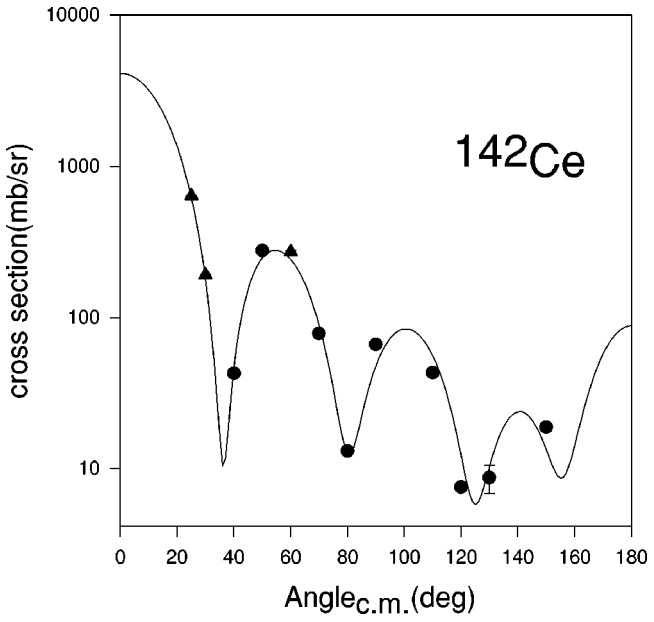

FIG. 4. Elastic scattering at 7.5 MeV from ^{142}Ce. The solid curve is an SOV calculation. The triangle points at small angles are taken from ^{140}Ce data, since at small angles the oxygen peak obscured the ^{142}Ce peak. The angular distributions for the two nuclei were equivalent at angles forward of 90°.

The total or combined uncertainties are represented by the error bars on the figures. For elastic scattering, errors are smaller than the points shown in Figs. 3 and 4.

III. MEAN FIELD DETERMINATION

The scattering potential was represented with the usual Woods-Saxon form factor for the real potential, and with the surface-peaked Woods-Saxon derivative form factor for the imaginary or absorptive potential [12]. Since ^{140}Ce is semimagic, the nuclei ^{140}Ce and ^{142}Ce are expected to be spherical, and hence the scattering field should be represented as spherical. This also means that direct coupling between elastic and inelastic scattering to low-lying collective levels would most likely be vibrational, with the first-order vibrational model (FOV) appropriate for the expected relatively weak coupling near magic numbers. But the FOV does not contain the modifications to the elastic scattering resulting from the direct coupling to excited levels. Therefore, to obtain the modest modifications of elastic scattering caused by coupling, all CC analyses in this work were done in the second order vibrational model (SOV).

The analyses were begun with the simpler SOM model, to obtain approximate values for potential strengths and geometries. The SOM calculations were carried out with the computer code OPSTAT-M, a modified form of the original OPSTAT code developed at Ohio University [13]. This original direct elastic scattering plus compound system cross sections code was here modified to OPSTAT-M to include the important level-width and resonance-resonance correlations required to provide correct statistical or compound system cross sections. The code includes compound system calculations for all excited levels known, and accommodates unresolved final states. The modified code has been extensively tested against other reliable compound system reaction codes.

Extensive work has been done evaluating mean fields for neutron scattering [7,14] in other nuclei. These prior analyses have included dispersion corrections [15,16] to the real scattering potentials which result from the presence of an absorptive potential. With these corrections one determines a real potential which extends to negative neutron energies to represent the bound single particle energies as well as the positive energy scattering amplitudes. The resulting potential strengths at low positive energies have weak energy dependencies, which gradually strengthen into the usual negative, approximately linear energy dependence as the neutron energy increases [7,17,18].

The first task in fixing the SOV potential as a function of energy is representing total cross sections as a function of energy over a rather wide range, as well as scattering properties at very low, or resonance neutron energies [6]. Since the methods used for obtaining neutron scattering potentials have been described many times [7,17–19], only the results are presented here. The real and absorptive potential parameters are presented as a function of neutron energy in Table I. The application of those potentials at the scattering energy of this experiment, 7.5 MeV, provided the parameters given for the SOV model in Table II. The SOM parameters, determined first, are also in Table II. The potential geometries given in Table II were used for both models throughout the full energy range of Table I.

These potentials enabled the representations of the total cross sections produced in Fig. 2. The resonance energy scattering properties include the *s*-wave resonance-averaged strength function s_0 as well as the scattering length extrapolated to zero energy, called R'. The parameter R' fixes the potential scattering away from resonances at very low energies, while s_0 is a resonance averaged property related primarily to the absorptive properties of the scattering potential at low energies. For ^{140}Ce, calculations give $s_0=1.37$ and $R'=5.9$ fm. The corresponding measured values are $s_0=1.1\pm0.3$ and 5.7 ± 0.2 fm, respectively [6]. The scattering potential must also represent the elastic scattering at the energy of this experiment, as shown in Figs. 3 and 4.

IV. DIRECT COUPLING—EXCITED LEVELS

Once the mean scattering field, as presented in Tables I and II, is well fixed it can be used as a basis for describing inelastic scattering through the coupling between the elastic and inelastic scattering channels. All calculations of direct inelastic scattering were done with the ECIS79 version of Raynal's coupled channels code [20]. This version of the code has been extensively tested through comparisons with other coupled channels codes.

Inelastic scattering cross sections to collective levels have two incoherent components. The interesting one comes from direct coupling between scattering channels, and the other is from decay of a compound system formed by neutron absorption, providing relatively weak cross section components compared to that of direct coupling. Direct coupling calcula-

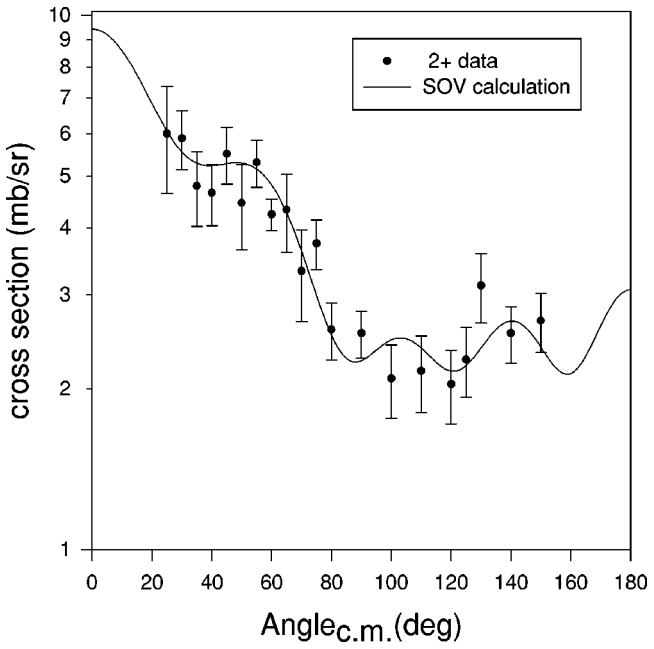

FIG. 5. Inelastic scattering to the 2_1^+ level of ^{140}Ce, with an SOV calculation.

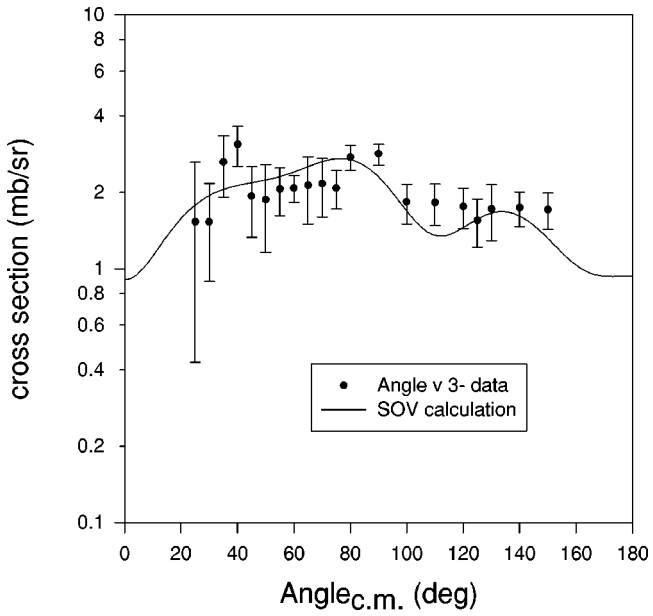

FIG. 6. Inelastic scattering to the 3^- level of ^{140}Ce, with an $E3$ SOV calculation.

tions were done for the levels of Fig. 1; the SOV was used for all couplings.

All SOV direct coupling calculations include also the weak compound absorption cross sections, or compound nucleus cross sections. These compound cross section calculations are approximated in ECIS79 with parameters which are set to reproduce the SOM calculated inelastic scattering cross sections, particularly for the unnatural parity states. It is useful to note that after the mean fields have been determined, the compound system calculations have no free parameters. The unnatural parity states have negligible coupling to elastic scattering, so their cross sections are entirely compound nucleus (i.e., nuclear absorption) cross sections. Thus the only free parameter in a CC calculation for a particular level is the strength of the coupling to that scattering amplitude.

^{140}Ce inelastic excitations. Measurements and calculations are presented in Fig. 5 for the 2_1^+ level of ^{140}Ce, and in Fig. 6 for the 3_1^- level. As can be seen, the calculated angular distributions reflect the data quite well. The calculations are normalized to the data through determination of the coupling parameter β_λ. The actual coupling strength is given by the product $\beta_\lambda R$, where R is the interaction radius. Since the (vibrational) coupling terms are obtained as derivatives of the real part of the scattering potential, it is the real radius which enters the coupling strength.

The 4_1^+ level of ^{140}Ce is of special interest because it is strongly excited in our scattering experiment, and because of the character of that excitation. Many low-lying levels of that nucleus are successfully represented in the QPM model. This model represents the 4_1^+ level entirely in terms of quasiparticle states, rather than as a level including significant multiphonon amplitudes.

Our representation of excitation of the 4_1^+ level is shown in Fig. 7. The dot-dash curve lying well below the experimental measurements would represent double phonon excitation, with a phonon strength implied by excitation of the 2_1^+ level. We see that this is completely inadequate to represent the measured excitation strength. The dash-double-dot curve represents a mixture of a one phonon 4^+ excitation

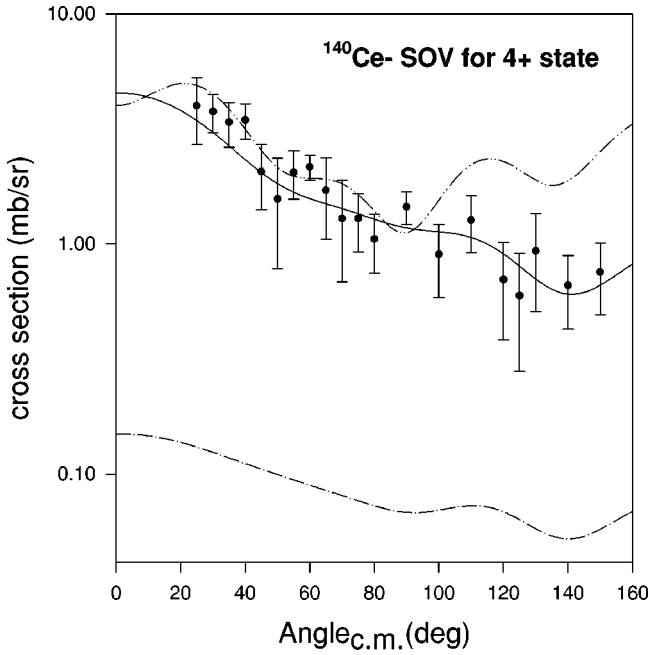

FIG. 7. Scattering to the 4_1^+ level of ^{140}Ce. The dot-dash curve is a two-phonon $E2$ excitation, with the 2^+ strength of Fig. 3 as the coupling strength for both phonons. The dash-double-dot curve is a mixed calculation, dominated by a single step $E4$ excitation and a 10% admixture of two-phonon $E2$ amplitude. The solid curve is a single step $E4$ excitation.

with just a few percent of double phonon amplitude. Any amount of double-phonon excitation mixed into the 4_1^+ amplitude destroys the fit to the data. The solid curve is the only satisfactory representation of all of the data; it arises from a pure $E4$, one phonon amplitude, the amplitude we would expect for a two-quasiparticle excitation. This calculation provides an excellent representation of the data, and tends to confirm that the QPM model provides the best representation for this nucleus. Also of note is that the $E4$ amplitude is unusually strong. This is consistent with the mixed two particle configurations presented [3] by W. Kim *et al.* The several two particle configurations could tend to give collectivity to this excitation stronger than that normally observed in scattering to 4^+ levels. The scattering cross section to this level is approximately double that found in scattering to 4^+ levels of nearby nuclei.

V. ISOSPIN MIXTURES IN TRANSITIONS TO COLLECTIVE EXCITATIONS

The proton and neutron excitation roles in individual collective levels can be separated by comparing the strength of exciting those levels by two different hadrons, or by one hadron and electromagnetic excitation. Several levels of ^{140}Ce have been excited in electron scattering [3], and the present experiment reveals the different strengths with which they are excited in neutron scattering. The comparison, then, of excitation strengths as observed in the electron scattering experiment and in this neutron scattering experiment will provide some information about the separate proton and neutron roles in a few levels of ^{140}Ce.

The one condition leading to probe independence of excitation is that both neutrons and protons of the target nuclei participate in the collective excitations with equal strengths on a per proton and per neutron basis. In that case, the excitation strengths, inferred from neutron and electron scattering, on a per nucleon basis, would be identical. Thus any departure from equality of matrix elements for different projectiles immediately means that protons and neutrons are involved in the excited level unequally.

According to calculations made in the QPM, excitations in neutron-magic ^{140}Ce can be treated as nearly pure proton excitations for the purposes of electron scattering [3]. Thus in this neutron scattering experiment, we might expect the matrix elements obtained from our experiment to be rather different than those obtained from electron scattering. As noted in earlier papers [19,21] and above, the coupling strengths which determine the inelastic scattering matrix elements are scaled according to the coupling expansion parameter $\beta R \equiv \delta$. The results from the electron scattering experiments cited [3], and our inelastic scattering strengths give the δ values of Table III for a few collective excited levels of ^{140}Ce.

The uncertainty of the extraction of δ^{em} is principally that of the cross section measured in the electron scattering measurements, since the mean field through which the electrons move is quite well determined. The mean field for neutron scattering is also well determined when one fits the many measured scattering properties. The uncertainties associated with inferred strengths for neutron scattering and electron scattering [3] are presented in Tables III and IV.

TABLE IV. Matrix element ratios for excitation of levels in ^{140}Ce. The δ_r values are coupling strengths determined in neutron scattering divided by those determined in electron scattering. The last column presents the matrix elements per nucleon for target neutrons divided by those for target protons. The departure of these ratios from 1 reflects the departure from isospin symmetry in the excitation of these collective levels.

	N/Z	δ_r	M_n/M_p	$(M_n/M_p)/(N/Z)$
^{140}Ce				
2^+	1.41	0.77 ± 0.06	0.40 ± 0.26	0.28 ± 0.19
3^-	1.41	0.71 ± 0.08	$0.13^{+0.37}_{-0.13}$	$\leqslant 0.34$
4_1^+	1.41	0.71 ± 0.12	$0.13^{+.53}_{-0.13}$	$\leqslant 0.5$

Combining these δ values enables us to extract the ratios M_n/N divided by M_p/Z, or the relative importance of neutrons and protons in the nuclear excitation. M_n denotes the matrix element for all neutrons in the target, while M_p is the same for target protons. N and Z are the numbers of neutrons and protons, respectively. The δ values are the coupling strengths on a per nucleon basis. Thus in electromagnetic excitation, the parameter yields $\delta^{em} = M_p/Z$. By convention, the reduced electromagnetic transition rate $B(E2) = (eM_p)^2$, for example, so that both M_p and M_n have the dimension of length, as does δ. The value of R as interaction radius for the electron scattering experiment is $R \approx 6$ fm [3], but by focusing on the full coupling strengths δ^{em} and $\delta^{n,n'}$, differences in the interaction radii for different experiments do not affect the strength comparisons.

For neutron scattering, we determine

$$\delta^{n,n'} = \frac{\chi_{np} M_p + \chi_{nn} M_n}{\chi_{np} Z + \chi_{nn} N},$$

where χ_{np} is a dimensionless parameter reflecting the effective, relative np interaction strength and χ_{nn} is one reflecting the nn interaction strength. Only ratios of these parameters will actually be important in the probe comparisons we make. Several previous studies [22,23] have introduced this method of separating the excitation roles of neutrons and protons in collective levels through probe independent excitation strengths. The above equation characterizes these separate roles in terms of the matrix elements for target proton excitations (M_p) and target neutron excitations (M_n) for the specific case of neutron scattering.

Bernstein *et al.* and authors cited therein [23], have compiled interaction strength ratios for several hadronic projectiles as a function of incident energy. They note that the ratio $\chi_r \equiv \chi_{np}/\chi_{nn} = 3.0$ is valid for nucleon energies below about 50 MeV. The ratios $\delta_r \equiv \delta^{n,n'}/\delta^{em}$ for the several levels of ^{140}Ce are then determined as

$$\delta_r = \frac{\chi_r M_p + M_n}{\chi_r Z + N} / (M_p/Z) = \frac{\chi_r + M_n/M_p}{\chi_r + N/Z}.$$

The δ ratios given in Table IV enable us to limit the sizes of the excitation matrix elements for protons and neutrons on a per nucleon basis, as shown in the last column of Table IV. Not surprisingly, the excitations observed in ^{140}Ce are dominated by proton excitations; target neutron strengths are small but present for the 2_1^+ level. They are less than 1/3 and 1/2 those of protons for the 3_1^- and 4_1^+ levels respectively. Protons dominate these ^{140}Ce excitations, as projected in the QPM model.

VI. SUMMARY

Our results for ^{140}Ce strongly support the general conclusion [3] that in the $N=82$ nuclei the 4_1^+ level, though with substantial collective strength, is almost exclusively a two-quasiparticle level. The strong excitation of the 4_1^+ level in our neutron scattering experiment could be consistent with constructive interference amongst the three particle configurations attributed to the level [3]. Our determinations of matrix elements for neutrons and protons M_n and M_p, for 2^+ and 3^- levels show that the excited levels are dominated, as expected, by proton excitations.

[1] R. K. J. Sandor *et al.*, Nucl. Phys. **A535**, 669 (1991).

[2] M. Grinberg and C. Stoyanov, Nucl. Phys. **A573**, 231 (1994).

[3] W. Kim, B. L. Miller, J. R. Calarco, L. S. Cardman, J. P. Connelly, S. A. Fayans, B. Frois, D. Goutte, J. H. Heisenberg, F. W. Hersman, V. Meot, T. E. Milliman, P. Mueller, C. N. Papanicolas, A. P. Platonov, V. Yu Ponomarev, and J. E. Wise, Phys. Rev. C **45**, 2290 (1992).

[4] W. Kim, J. R. Calarco, J. P. Connelly, J. H. Heisenberg, F. W. Hersman, T. E. Milliman, J. E. Wise, B. L. Miller, C. N. Papanicolas, V. Yu Ponomarev, E. E. Saperstein, and A. P. Platonov, Phys. Rev. C **44**, 2400 (1991).

[5] R. E. Schenter and F. Schmittroth, ENDFB/VI Library, 1974.

[6] S. F. Mughabghab, M. Divadeenam, and N. E. Holden, *Neutron Cross Sections* (Academic, New York, 1981) Vol. 1, Part A, Z = 1–60.

[7] Sally F. Hicks, J. M. Hanly, S. E. Hicks, G. R. Shen, and M. T. McEllistrem, Phys. Rev. C **49**, 103 (1994).

[8] S. Pearlstein, ENDF/B-VI Library, 1992; G. Houat, J. Lachkar, J. Sigaud, and Y. Patin, Service de Physique et Techniques Nucléaires, Centre d'Etudes de Bruyères-le-Châtel, Report No. CEA-N-2080, 1979 (unpublished).

[9] R. L. Schulte, M. Cosack, A. W. Obst, and J. L. Weil, Nucl. Phys. **A192**, 609 (1972); H. Liskien and A. Paulsen, Nucl. Data Tables **11**, 569 (1973).

[10] J. D. Brandenberger and T. B. Grandy, Nucl. Instrum. Methods **93**, 495 (1971).

[11] D. E. Velkley, D. W. Glasgow, J. D. Brandenberger, and M. T. McEllistrem, Nucl. Instrum. Methods **129**, 231 (1975); John R. Lilley, Internal Report No. P2N/934/80, Service de Physique et Techniques Nucléaires, Centre d'Études de Bruyères-le-Châtel, 1980.

[12] G. R. Satchler, *Direct Nuclear Reactions* (Oxford University Press, New York, 1983), p. 456ff.

[13] J. R. M. Annand, Ohio University report, 1984 (unpublished). (Available in original form from R. W. Finlay, Physics Department, Ohio University, Athens, Ohio. Available as modified from M. T. McEllistrem, Physics Department, University of Kentucky.)

[14] S. E. Hicks, Z. Cao, M. Mirzaa, J. L. Weil, J. M. Hanly, Sally F. Hicks, and M. T. McEllistrem, Phys. Rev. C **40**, 2509 (1989).

[15] C. Mahaux and H. Ngo, Phys. Rev. Lett. **100B**, 285 (1981).

[16] C. Mahaux, H. Ngo, and G. R. Satchler, Nucl. Phys. **A449**, 354 (1986); C. Mahaux and R. Sartor, Phys. Rev. Lett. **57**, 3015 (1986); Nucl. Phys. **A458**, 25 (1986).

[17] S. E. Hicks and M. T. McEllistrem, Phys. Rev. C **37**, 1787 (1988).

[18] C. H. Johnson, D. J. Horen, and C. Mahaux, Phys. Rev. C **36**, 2252 (1987).

[19] T. B. Clegg, G. Haouat, J. P. Delaroche, Ch. Lagrange, J. Chardine, S. E. Hicks, G. R. Shen, and M. T. McEllistrem, Phys. Rev. C **40**, 2527 (1989).

[20] J. Raynal, Report No. ECIS79 (unpublished); *Computing as a Language of Physics* (IAEA, Vienna, 1972), p. 75; Phys. Rev. C **23**, 2571 (1981).

[21] D. J. Horen, R. L. Auble, F. E. Bertrand, M. L. Halbert, G. R. Satchler, M. Theonnessen, R. L. Varner, V. R. Brown, P. L. Anthony, and V. A. Madsen, Phys. Rev. C **44**, 128 (1991).

[22] V. A. Madsen, V. R. Brown, and J. D. Anderson, Phys. Rev. C **12**, 1205 (1975).

[23] A. M. Bernstein, V. R. Brown, and V. A. Madsen, Phys. Lett. **103B**, 255 (1981); Comments Nucl. Part. Phys. **11**, 203 (1983).